J|A|C|S
COMMUNICATIONS

Published on Web 03/16/2004

Absolute Structural Constraints on Amyloid Fibrils from Solid-State NMR Spectroscopy of Partially Oriented Samples

Nathan A. Oyler and Robert Tycko*

Laboratory of Chemical Physics, National Institute of Diabetes and Digestive and Kidney Diseases, National Institutes of Health, Building 5, Room 112, Bethesda, Maryland 20892-0520

Received December 15, 2003; E-mail: robertt@niddk.nih.gov

Amyloid fibrils are filamentous aggregates formed by a variety of disparate peptides and proteins. The molecular structures of amyloid fibrils are of current interest due to their involvement in amyloid diseases,[1] as well as fundamental mechanistic and physical chemical issues about amyloid formation.[2] Solid-state nuclear magnetic resonance (NMR) methods are particularly useful in structural studies of amyloid fibrils because these methods provide site-specific molecular-level structural constraints without requiring crystallinity or solubility. To date, structurally significant solid-state NMR parameters (e.g., dipole−dipole couplings, isotropic chemical shifts, and spin interaction tensor correlations) have been obtained exclusively from unoriented (i.e., isotropic powder) fibril samples.[3−6] Here we demonstrate that complementary information can be obtained from measurements on partially oriented samples. Specifically, we show that the direction of the fibril axis relative to a carbonyl ^{13}C chemical shift anisotropy (CSA) tensor (i.e., a locally defined, molecule-fixed, principal axis system) can be determined from magic-angle spinning (MAS) sideband patterns in ^{13}C NMR spectra of fibrils deposited on planar substrates. The fibril axis direction determined in this way relative to the carbonyl CSA tensor of Val12 in fibrils formed by the 40-residue β-amyloid peptide associated with Alzheimer's disease (Aβ_{1-40}) agrees well with the predictions of a recent structural model.[6]

Figure 1 indicates the conceptual design of the experiment. Assuming that all peptide molecules within a fibril are related by rotation about the long fibril axis (consistent with the characteristic drill-like morphologies of amyloid fibrils[6,7]), the fibril axis direction with respect to the CSA tensor at a single ^{13}C-labeled site is defined by angles θ and ϕ. Because amyloid fibrils typically exhibit ∼10 nm diameters and ∼0.1−10 μm lengths, deposition on a planar substrate should create a highly anisotropic distribution of fibril orientations (hence, CSA tensor orientations), with most fibrils lying nearly in the substrate plane. In a MAS NMR spectrum, the anisotropic orientational distribution gives rise to distorted spinning sideband patterns, from which the distribution relative to the MAS rotor (and ultimately θ and ϕ) can be inferred.[8] Different spinning sideband patterns are expected when the substrate is placed either parallel (∥) or perpendicular (⊥) to the MAS rotor axis.

Films of Aβ_{1-40} fibrils, synthesized with ^{13}C labels at the carbonyl site of Val12 and the α-carbon site of Gly9, were cast from aqueous solution onto mica substrates. Experimental ^{13}C MAS spectra are presented in Figure 2, along with corresponding best-fit simulations. Differences between the spectrum in Figure 2A (⊥) and the spectra in Figure 2B (∥) indicate that deposition on mica indeed generates an anisotropic orientational distribution. Most notably, the most intense peak in Figure 2A is the +1 sideband, while the most intense peaks in Figure 2B are the centerbands. Spectra in Figure 2B vary with the rotor phase at the start of signal acquisition and exhibit partially dispersive line shapes because the orientational distribution is not symmetric about the MAS rotor axis.[9]

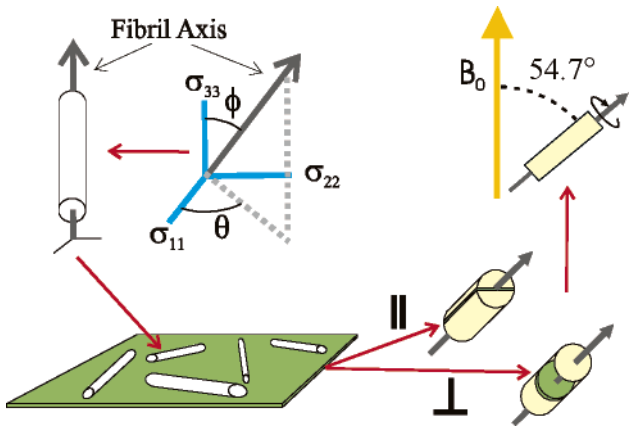

Figure 1. Experimental design. The direction of the long axis of the amyloid fibrils relative to the CSA principal axis system of a ^{13}C-labeled site is defined by θ and ϕ. When deposited on mica, fibrils lie preferentially in a plane, creating a highly anisotropic orientational distribution. Mica sheets are placed in a MAS rotor either parallel (∥) or perpendicular (⊥) to the rotor axis, and ^{13}C NMR spectra are obtained under MAS. Values of θ and ϕ, which represent constraints on the molecular structure of the fibrils, are determined by comparison of experimental and simulated spinning sideband patterns.

Spinning sideband patterns were simulated as a function of θ and ϕ with a C++ program running in the Matlab environment. Simulations included ∼25000 fibril orientations, with the long axis within ±5° of the substrate plane. Larger deviations from co-planarity produced poorer agreement with experiments, validating the picture in Figure 1. Full rotational disorder about the fibril axis and about the direction normal to the substrate plane was assumed. Val12 carbonyl CSA principal values were determined from MAS spectra of an unoriented fibril sample.

Figure 3 presents contour plots of the reduced χ^2 deviation between experimental spectra in Figure 2 and simulations. θ and ϕ are only plotted from 0° to 90° because of symmetry with respect to reversal of the fibril axis direction and the following paired symmetries between the crystallite orientation defined by Euler angles (α,β,γ) and the fibril axis direction defined by (θ,ϕ): [(α,β,γ), θ] ↔ [($\pi-\alpha$,$\pi-\beta$,$\pi+\gamma$),$\pi-\theta$] and [(α,β,γ), ϕ] ↔ [(-α,$\pi-\beta$,$\pi+\gamma$),$\pi-\phi$]. Notably, the ∥ and ⊥ spectra contain independent information, as seen by the different patterns of local minima in Figure 3, A and B. Asterisks in Figure 3 indicate the fibril axis direction predicted by a recent atomic model for the Aβ_{1-40} fibril structure derived from solid-state NMR and electron microscopy data,[6a] in which Val12 is contained in a parallel β-sheet within the "cross-β" motif characteristic of amyloid structures.[2,10] The asterisks are located near a χ^2 minimum common to both sample orientations, indicating good agreement between the model and the present

10.1021/ja031719k

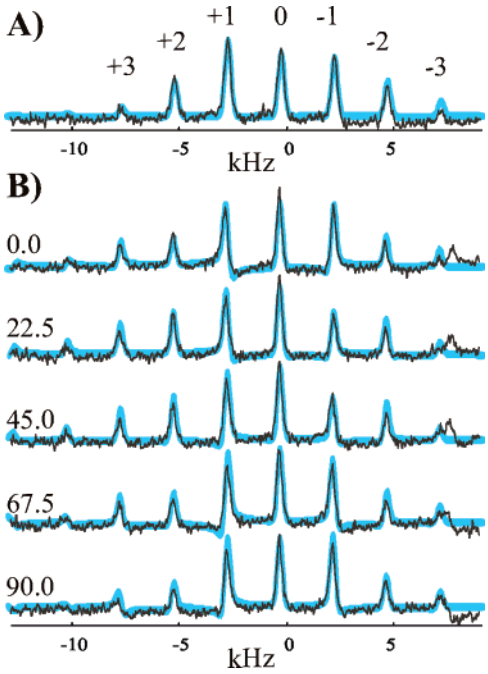

Figure 2. (A) Experimental ^{13}C MAS NMR spectrum (thin black line) and best-fit simulation (thick blue line) for Aβ_{1-40} fibrils on mica in the ⊥ geometry. Numbers above the spectrum indicate the spinning sideband lines for the ^{13}C-labeled Val12 carbonyl. (B) Experimental spectra and best-fit simulations in the || geometry, for indicated values of the MAS rotor phase at the start of signal acquisition. All spectra acquired at 100.4 MHz ^{13}C NMR frequency and 2.5 kHz MAS frequency. Sample in (A) was 2.5 mg Aβ_{1-40} on ~50 mica pieces, 2.5 mm × 2.5 mm × 25 μm each. Sample in (B) was 7.5 mg Aβ_{1-40} on ~30 mica pieces, 12 mm × 2.5 mm × 25 μm each. Peaks at the far right are sidebands from the ^{13}C-labeled α-carbon of Gly9.

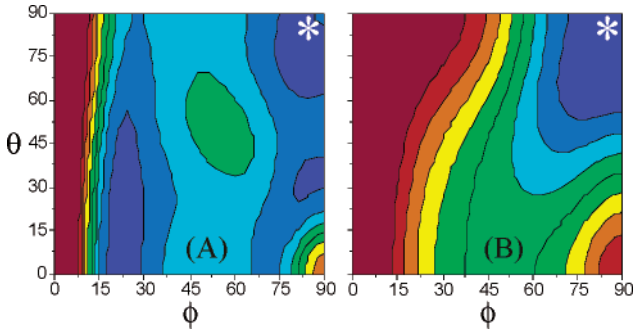

Figure 3. Contour plots of the reduced $\chi^2(\theta,\phi)$ for fits to spectra in Figure 2A (⊥) and Figure 2B (||). Darkest blue represents $\chi^2(\theta,\phi) < 2.0$. Contour level increment is 0.5. Dark red represents $\chi^2(\theta,\phi) > 5.5$. In (B), spectra for all rotor phases were fit simultaneously.

experiments. The combined best-fit values are $(\theta,\phi) = (69°,81°)$, implying an angle of 19° between the Val12 C═O bond and the fibril axis (assuming a standard CSA tensor[11]). On the basis of Monte Carlo simulations, the uncertainty in both θ and ϕ is approximately ±10° for the level of noise in the spectra of Figure 2.

Although mica sheets are atomically flat, thin, and durable and contribute no ^{13}C NMR background, their large magnetic susceptibility (presumably due to iron oxide impurities) produces a rotor phase dependent, but nearly uniform, shift of the ^{13}C NMR frequencies in the || geometry. Good agreement between experiments and simulations was achieved only after calibrating this shift and including it in simulations.

Experiments described above, while similar to experiments performed on silk fibers,[8d-f] differ from all previous solid-state NMR measurements on amyloid fibrils in that constraints are obtained on the absolute orientation of a single chemical group within the overall morphology of the supramolecular structure, rather than on distances between or relative orientations of two groups with no direct connection to the overall morphology. The success of these experiments sets the stage for the development of additional solid-state NMR techniques to measure the absolute orientation of particular chemical bonds in partially oriented samples, as well as techniques applicable to samples with uniformly labeled residues.

Supporting Information Available: (1) Additional details of sample preparation, NMR experiments and simulations. (2) Experimental spectra of unfibrillized Aβ_{1-40} on mica and simulations for an isotropic orientational distribution. (3) Characterization of the dependence of the mica susceptibility shift on MAS rotor phase. This material is available free of charge via the Internet at http://pubs.acs.org.

References

(1) Sipe, J. D. *Annu. Rev. Biochem.* **1992**, *61*, 947−975.
(2) Tycko, R. *Biochemistry* **2003**, *42*, 3151−3159.
(3) (a) Lansbury, P. T.; Costa, P. R.; Griffiths, J. M.; Simon, E. J.; Auger, M.; Halverson, K. J.; Kocisko, D. A.; Hendsch, Z. S.; Ashburn, T. T.; Spencer, R. G. S.; Tidor, B.; Griffin, R. G. *Nat. Struct. Biol.* **1995**, *2*, 990−998. (b) Jaroniec, C. P.; MacPhee, C. E.; Astrof, N. S.; Dobson, C. M.; Griffin, R. G. *Proc. Natl. Acad. Sci. U.S.A.* **2002**, *99*, 16748−16753.
(4) (a) Benzinger, T. L. S.; Gregory, D. M.; Burkoth, T. S.; Miller-Auer, H.; Lynn, D. G.; Botto, R. E.; Meredith, S. C. *Proc. Natl. Acad. Sci. U.S.A.* **1998**, *95*, 13407−13412. (b) Benzinger, T. L. S.; Gregory, D. M.; Burkoth, T. S.; Miller-Auer, H.; Lynn, D. G.; Botto, R. E.; Meredith, S. C. *Biochemistry* **2000**, *39*, 3491−3499.
(5) (a) Antzutkin, O. N.; Balbach, J. J.; Leapman, R. D.; Rizzo, N. W.; Reed, J.; Tycko, R. *Proc. Natl. Acad. Sci. U.S.A.* **2000**, *97*, 13045−13050. (b) Balbach, J. J.; Ishii, Y.; Antzutkin, O. N.; Leapman, R. D.; Rizzo, N. W.; Dyda, F.; Reed, J.; Tycko, R. *Biochemistry* **2000**, *39*, 13748−13759. (c) Balbach, J. J.; Petkova, A. T.; Oyler, N. A.; Antzutkin, O. N.; Gordon, D. G.; Meredith, S. C.; Tycko, R. *Biophys. J.* **2002**, *83*, 1205−1216. (d) Tycko, R.; Ishii, Y. *J. Am. Chem. Soc.* **2003**, *125*, 6606−6607. (e) Antzutkin, O. N.; Balbach, J. J.; Tycko, R. *Biophys. J.* **2003**, *84*, 3326−3335.
(6) (a) Petkova, A. T.; Ishii, Y.; Balbach, J. J.; Antzutkin, O. N.; Leapman, R. D.; Delaglio, F.; Tycko, R. *Proc. Natl. Acad. Sci. U.S.A.* **2002**, *99*, 16742−16747. (b) Antzutkin, O. N.; Leapman, R. D.; Balbach, J. J.; Tycko, R. *Biochemistry* **2002**, *41*, 15436−15450.
(7) (a) Goldsbury, C. S.; Wirtz, S.; Muller, S. A.; Sunderji, S.; Wicki, P.; Aebi, U.; Frey, P. *J. Struct. Biol.* **2000**, *130*, 217−231. (b) Jimenez, J. L.; Nettleton, E. J.; Bouchard, M.; Robinson, C. V.; Dobson, C. M.; Saibil, H. R. *Proc. Natl. Acad. Sci. U.S.A.* **2002**, *99*, 9196−9201.
(8) (a) Harbison, G. S.; Spiess, H. W. *Chem. Phys. Lett.* **1986**, *124*, 128−134. (b) Glaubitz, C.; Watts, A. *J. Magn. Reson.* **1998**, *130*, 305−316. (c) Lee, S. A.; Grimm, H.; Pohle, W.; Scheiding, W.; van Dam, L.; Song, Z.; Levitt, M. H.; Korolev, N.; Szabo, A.; Rupprecht, A. *Phys. Rev. E: Stat. Phys., Plasmas, Fluids, Relat. Interdiscip. Top.* **2000**, *62*, 7044−7058. (d) Demura, M.; Yamazaki, Y.; Asakura, T.; Ogawa, K. *J. Mol. Struct.* **1998**, *441*, 155−163. (e) Nicholson, L. K.; Asakura, T.; Demura, M.; Cross, T. A. *Biopolymers* **1993**, *33*, 847−861. (f) van Beek, J. D.; Hess, S.; Vollrath, R.; Meier, B. H. *Proc. Natl. Acad. Sci. U.S.A.* **2002**, *99*, 10266−10271.
(9) (a) Maricq, M. M.; Waugh, J. S. *J. Chem. Phys.* **1979**, *70*, 3300−3316. (b) Munowitz, M. G.; Griffin, R. G. *J. Chem. Phys.* **1982**, *76*, 2848−2858.
(10) Sunde, M.; Blake, C. C. F. *Q. Rev. Biophys.* **1998**, *31*, 1−39.
(11) Oas, T. G.; Hartzell, C. J.; McMahon, T. J.; Drobny, G. P.; Dahlquist, F. W. *J. Am. Chem. Soc.* **1987**, *109*, 5956−5962.

JA031719K